magnetochemistry

MDPI

Article

Magnetic Adsorbent Based on Faujasite Zeolite Decorated with Magnesium Ferrite Nanoparticles for Metal Ion Removal

Mariana Rodrigues Meirelles [1,2], João Otávio Donizette Malafatti [1,3,*], Márcia Tsuyama Escote [4], Alexandre Henrique Pinto [5] and Elaine Cristina Paris [1,*]

1 National Nanotechnology Laboratory for Agriculture (LNNA), Embrapa Instrumentação, XV de Novembro St., 1452, São Carlos 13560-970, SP, Brazil
2 Institute of Chemistry, University of São Paulo, Av. Trab. São Carlense, 400, São Carlos 13566-590, SP, Brazil
3 Department of Chemistry, Federal University of São Carlos, Rod. Washington Luís, Km 235, São Carlos 13565-905, SP, Brazil
4 Center for Engineering, Modeling and Applied Social Sciences (CECS), Federal University of ABC (UFABC), Avenida dos Estados, 5001, Santo André 09210-170, SP, Brazil
5 Department of Chemistry and Biochemistry, Manhattan College, 4513, Riverdale, New York, NY 10471, USA
* Correspondence: jmalafatti@hotmail.com (J.O.D.M.); elaine.paris@embrapa.br (E.C.P.); Tel.: +55-16-2107-2868 (E.C.P.)

Abstract: Magnetic nanoparticles are a promising alternative as a support in adsorption processes, aiming at the easy recovery of the aqueous medium. A faujasite zeolite (FAU) surface was decorated with magnesium ferrite ($MgFe_2O_4$) nanoparticles. FAU is a porous adsorbent with high specific surface area (SSA) and chemical stability. The FAU:$MgFe_2O_4$ nanocomposite 3:1 ratio (w w^{-1}) promotes the combination of the surface and magnetic properties. The results showed the effectiveness of the $MgFe_2O_4$ immobilization on the FAU surface, exhibiting a high SSA of 400 m^2 g^{-1}. The saturation magnetization (Ms) was verified as 5.9 emu g^{-1} for $MgFe_2O_4$ and 0.47 emu g^{-1} for FAU:$MgFe_2O_4$, an environmentally friendly system with soft magnetic characteristics. The magnetic nanocomposite achieved high adsorption values of around 94% removal for Co^{2+} and Mn^{2+} ions. Regarding its reuse, the nanocomposite preserved adsorption activity of above 65% until the third cycle. Thus, the FAU:$MgFe_2O_4$ nanocomposite presented favorable adsorptive, magnetic, and recovery properties for reuse cycles in polluted water.

Keywords: magnetic nanocomposite; magnesium ferrite; faujasite zeolite; adsorption; metal ions

Citation: Meirelles, M.R.; Malafatti, J.O.D.; Escote, M.T.; Pinto, A.H.; Paris, E.C. Magnetic Adsorbent Based on Faujasite Zeolite Decorated with Magnesium Ferrite Nanoparticles for Metal Ion Removal. *Magnetochemistry* **2023**, *9*, 136. https://doi.org/10.3390/magnetochemistry9050136

Academic Editor: Karim Zehani

Received: 23 March 2023
Revised: 6 May 2023
Accepted: 18 May 2023
Published: 20 May 2023

1. Introduction

In recent decades, environmental pollution has become a worldwide challenge for global society due to the various adverse effects caused in different ecosystems [1]. Environmental degradation creates constraints on natural resources, negatively impacting the conditions of life on Earth [2,3]. Inorganic pollutants have been found frequently in water supplies [4]. Typical contaminants found in wastewater are toxic metals, such as iron (Fe), nickel (Ni), lead (Pb), cobalt (Co), manganese (Mn), and cadmium (Cd), among others [5]. In high concentrations, these cations can cause irreversible damage to the body's functioning, sometimes leading to death [6].

In this scenario, decontaminating/recovering polluted aquatic environments, minimizing waste production, and avoiding inadequate disposal are essential points for conserving this vital resource [7]. There are several processes for removing toxic metal ions in aqueous media, such as coagulation-flocculation [8], complexation [9], chemical precipitation [10], electrochemical treatment [11], and adsorption [12]. The adsorption process is one of the most effective methods for this application due to its high efficiency, low cost, and capacity to use in many cycles. However, factors such as adsorbate surface area, pore size distribution, chemical nature, temperature, and concentration of the components can interfere

with the adsorption process [13]. Additionally, exploring the intrinsic structure materials elucidates the improved properties of nanoparticles [14].

Zeolites stand out as a promising adsorbent due to high surface area values, regularity in pore size distribution, selectivity, and ion exchange capacity [15,16]. Zeolites are hydrated aluminosilicates with a structure accommodating sodium, potassium, and calcium ions. The tetrahedrons $[SiO_4]$ and $[AlO_4]^-$ form the zeolite crystal lattice [17]. The high surface area comes from the microporous structures formed due to the union of tetrahedrons. The tetrahedra grouping can occur in different ways, giving rise to different types of zeolites [18]. Faujasite (FAU) group zeolites have interesting properties for the adsorption process, such as high pore volume, empty intercrystalline space, and several acidic sites on the structure's outer surface [19,20]. The FAU zeolites present a cubic symmetry structure with pores arranged perpendicularly with a diameter of 7.4 Å [21]. The different faujasite structures depend on the SiO_2/Al_2O_3 molar ratio. A smaller Si/Al ratio supplies a more significant negative charge on the system, balanced by cations in non-structural positions. Thus, cation exchange processes are an essential property of zeolites [22].

One of the significant challenges of using the adsorbent systems is adequate immobilization to present efficient removal and reuse, maintaining efficacy in many cycles [23,24]. Magnetic adsorbents are an alternative that promote the easy adsorption of pollutants with practical posterior separation from effluents using a magnetic field [25–29]. Ferrites are double oxides of iron and another metal of the general formula Mfe_2O_4, where M is a bivalent metal element (usually, Mn^{2+}, Fe^{2+}, Zn^{2+}, Co^{2+}, Ni^{2+}, Cu^{2+}, or Mg^{2+}), generally in a spinel-type structure [1,30]. Ferrites can be synthesized for different applications, such as sol-gel [31], coprecipitation [32], combustion [33], hydrothermal [34], and microwave [35], by controlling the diameter, phase structure, and morphology, as well as the magnetic properties. The synergism between magnetic and electronic properties allows the possibility of ferrite application in batteries [36], sensors [37], solar cells [38], adsorption [39], and catalysis [24].

Magnesium ferrite ($MgFe_2O_4$) is attractive due to its magnetic behavior and high specific surface area (SSA) in a non-toxicity material, maintaining desirable properties and environmentally friendly aspects. In the $MgFe_2O_4$ spinel structure, the Fe^{3+} ions are homogeneously distributed between the octahedral and tetrahedral sites [40]. Therefore, the $MgFe_2O_4$ magnetic point occurs due to uncompensated iron spins distributed in the system [41]. Nonkumwong and colleagues [42] synthesized $MgFe_2O_4$-Au nanoparticles and studied the in vitro cytotoxicity response. The nanocomposites obtained did not exhibit cytotoxicity in the test performed on mammalian cells in vitro. In this sense, the $MgFe_2O_4$ compound presents magnetic behavior, promoting the removal after application with a magnetic field, permitting the system recovery and reuse in an environmentally friendly way.

Magnetic zeolites can potentially remove toxic ions from contaminated water. Peng and coworkers [43] obtained magnetic FAU from molybdenum and iron II/III oxides ore. The material showed high efficiency in removing cadmium (204.2 mg g^{-1}) ions in wastewater. The authors also found that ion exchange is the magnetic zeolite's primary mechanism of cadmium adsorption. In a study using naturally activated zeolites and Fe_3O_4, the authors evaluated the removal of chromium ions from contaminated water [44]. The results indicated a compound with high efficiency and competitiveness in removing chromium ions (84–99%). Mthombeni and colleagues [45] evaluated the remotion of chromium ions using a magnetic natural zeolite–polymer composite, finding that the system could remove up to 99.99% of the contaminant at an ideal pH. In this way, the magnetic nanocomposite based on zeolites with ferrites shows promising results in polluted water environmental remediation.

To our knowledge, the better elucidation concerning the adsorption of toxic metal ions using the FAU zeolite decorated with magnesium ferrite nanoparticles is essential for environmental remediation science. The proposed system (FAU:$MgFe_2O_4$) was not found in the current literature, since magnesium ferrite is an alternative as a low-toxicity

compound composed of Fe and Mg ions, both nutrients for the soil. Thus, the present work aimed to obtain a porous magnetic nanocomposite from immobilizing magnesium ferrite nanoparticles on the FAU zeolite surface to perform the adsorption and reuse of toxic metal ions, such as Co^{2+} and Mn^{2+}.

2. Materials and Methods

2.1. Synthesis

2.1.1. FAU Zeolite Synthesis

Faujasite zeolite (FAU) was obtained by the sol-gel process followed by hydrothermal treatment adapted from Romero [19]. The reagents used were Silica (Tixosil® 333, donated by Evonik Degussa, Essen, Germany), the mineralizing NaOH (Synth), and Sodium Aluminate (Sigma Aldrich, St. Louis, MI, USA), as sources of Si, Na, and Al, respectively. First, a sodium aluminate solution was prepared in 50 mL of deionized water. Next, 50 mL of a NaOH solution (2.7 M) was added under magnetic stirring at room temperature. After that, the colloidal silica was progressively added until a gel formed. The viscous gel remained in static, aging for 24 h on a bench at room temperature. Then, the gel underwent hydrothermal treatment at 100 °C for 2 h. Finally, the material was centrifuged at 10,000 rpm to neutralize the solution and was dried in a circulating air oven at 60 °C for 24 h.

2.1.2. Magnesium Ferrite Synthesis

Magnesium ferrite was adapted from the method by Omer et al. [46]. The starting reagents were $FeCl_3 \cdot 6H_2O$ (Synth) and $MgCl_2 \cdot 6H_2O$ (Synth). First, each salt precursor was solubilized in 25 mL water, resulting in a solution of 0.4 mol L^{-1}. After the solubilization, the solutions were mixed to complete homogenization. Then, the 25 mL NaOH solution (3 mol L^{-1}) was kept under constant stirring. The resulting suspension was washed and centrifuged at 8000 rpm for 10 min. Finally, the resulting material was dried in a circulating air oven. Ultimately, the ferrite calcination was carried out in an EDG 3000 muffle furnace. The thermal treatment was performed using heating to 300 °C for 4 h (controlled organic elimination), with subsequent treatment at 500 °C for 2 h to obtain magnetic ferrite.

2.1.3. FAU:Ferrite Nanocomposite Synthesis—FAU:$MgFe_2O_4$(3:1)

The anchoring of $MgFe_2O_4$ nanoparticles on the faujasite zeolite (FAU) surface was based on Yamaura [47]. Initially, FAU was suspended in deionized water and mixed with $MgFe_2O_4$ at a 3:1 (w w^{-1}) ratio of the FAU:$MgFe_2O_4$ nanocompound. Next, the process was completed using an ultrasonic tip at a 20% amplitude for 30 min in an ice bath. After complete dispersion and homogenization, the obtained composite was centrifuged at 8000 rpm for 5 min and then dried in an oven at 60 °C for 12 h. Finally, the nanocomposite was calcinated in the conditions to obtain the magnetic $MgFe_2O_4$ described in Section 2.1.2.

2.2. Characterization Techniques

The structural analysis of the compounds was performed through X-ray diffraction. The equipment used was Shimadzu XRD-6000, operating with Cu-Kα radiation, λ 1.5406 Å at 1 °C min^{-1} from 2θ 5° to 80°. The images were obtained via scanning electron microscopy (SEM) equipment, JEOL® model 6701F, using at 5 kV. The samples were also analyzed through energy dispersive spectroscopy (EDS) at 132 eV resolution in a model 6742[a] Ultradry Silicon Drift Detector. For specific surface area analysis, N_2 physisorption/desorption was performed using the Brunauer, Emmett, and Teller (BET) method. In addition, the magnetic properties of magnesium ferrites ($MgFe_2O_4$) and the nanocomposite were evaluated through magnetic curves via an optical magnetizer (Model PPMS 9 Evercool—Quantum Design) at room temperature (300 K) and with a magnetic field between −20,000 to 20,000 Oe.

2.3. Adsorption Experiments

For the kinetic assays, the conditions of 1.0 g L^{-1} for FAU:$MgFe_2O_4$ (3:1) and 10 mg L^{-1} for each ion (Co^{2+} and Mn^{2+}) were established. Likewise, the composite was previously weighed, and the ion solution was added mechanically. Then, the adsorption tests were carried out at 15, 30, 45, 60, 120, 180, 240, 300, 360, 480, and 960 min. Afterward, the material was centrifuged, and 2 mL aliquot was used for atomic absorption spectrometry analysis. Finally, the adsorbed percentage amount of each ion at different times was determined.

The percentage of removal for each ion was calculated through the following equation:

$$Removal\ (\%) = \frac{c_i - c_f}{c_i} \times 100 \quad (1)$$

The adsorption capacity of the adsorbent for each ion as a function of time, qt (mg g^{-1}), was determined according to the following equation:

$$qt = \frac{Ci - Ct}{m} V \quad (2)$$

where *Removal* % (mg L^{-1}) is the amount (percentage adsorbed by each ion), Ci is the initial ions concentration (mg L^{-1}), c_f is the the final concentration of the ions still present in the solution, and Ct (mg L^{-1}) is the concentration of ions remaining in the solution at time t (h). The experiments were conducted at pH 7 and room temperature (25 °C).

The kinetic models of pseudo-first and pseudo-second order were evaluated. The equations of the parameters of these models are presented below:

$$\text{Pseudo-First Order kinetic model: } qt = qe\left(1 - e^{-k_1 t}\right) \quad (3)$$

where qe is the equilibrium constant (mg g^{-1}) and k_1 is the rate constant (min^{-1}).

$$\text{Pseudo-Second Order kinetic model: } qt = \frac{t}{\left(\frac{1}{k_2 q_e^2}\right) + \frac{t}{q_e}} \quad (4)$$

where k_2 is the constant rate (g mg^{-1} min^{-1}).

For the reuse test, the conditions of 1.0 g L^{-1} of FAU: $MgFe_2O_4$ and 0.01 g L^{-1} for each ion (Co^{2+}, Mn^{2+}) were fixed. The tests were performed in triplicate. Initially, aliquots of the aqueous solutions were added into flasks containing the previously weighed nanocomposites, as described for the adsorption assays. The flasks remained in mechanical agitation for 24 h and were then recovered. Then, the aliquots of the supernatant solution were removed and atomic absorption spectrometry analysis was performed. The centrifugation was carried out in the laboratory to minimize equipment damage due to the presence of particles.

Next, a fresh 0.01 g L^{-1} solution of the cations was added to the same vial containing the adsorbent. After 24 h, the flask was separated and an aliquot was taken for analysis. This reuse process was conducted in three cycles. Then, the adsorbed percentage amount of individual ions was obtained by Equation (1).

2.4. Magnetical Recovery

The mass recovery was evaluated to verify the nanocomposite capacity to be attracted by a magnetical field. First, FAU:$MgFe_2O_4$ (0.1 g) was inserted in a water flask. After stabilization in ambient temperature for 30 min, a neodymium magnet was utilized for separation from the aqueous medium. Next, the material was washed with ethanol alcohol and dried at 80 °C for mass determination on an analytical scale. Thereafter, the system (FAU:$MgFe_2O_4$) was resuspended in water, and the process was repeated five times.

3. Results

The structural properties of the individual synthesized compounds and the FAU:$MgFe_2O_4$ nanocomposite were evaluated. The XRD patterns are illustrated in Figure 1 to assess the synthesized materials' phase formation and structure.

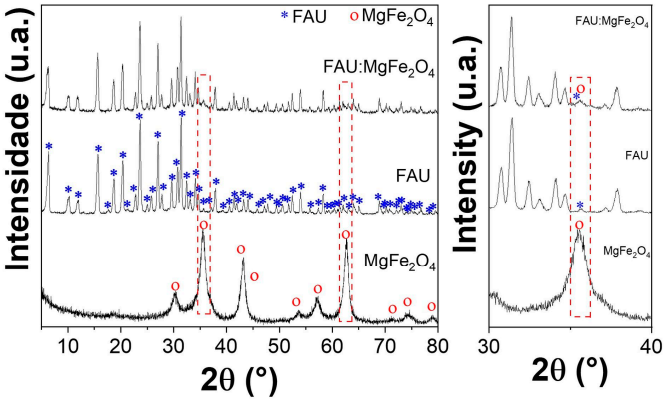

Figure 1. X-ray diffraction analyses for FAU, $MgFe_2O_4$, and FAU:$MgFe_2O_4$ (3:1) on the left and the high magnification on the right.

The synthesized zeolite showed characteristic peaks of the faujasite phase, according to the JCPDS data sheet 043-0168. For the synthesized $MgFe_2O_4$, all peaks correspond to the JCPDS number 71–1232. No additional peaks were observed. The results obtained by XRD evidenced the crystallinity and purity of the precursors for the nanocomposite production. In the FAU:$MgFe_2O_4$ (3:1) diffractogram, the FAU phase maintenance can be observed. Regarding the $MgFe_2O_4$ reflections, the FAU peak superposition makes it difficult to verify whether the ferrite phase was retained. However, the red highlights and the graph magnification (Figure 1 right) confirm the presence of the most intense $MgFe_2O_4$ peak in the composite. Thus, the presence of FAU and $MgFe_2O_4$ in the obtained nanocomposite is evident. Similar research on magnetic nanocomposites has shown the synthesis of $MgFe_2O_4$ nanocomposite without any structural change in the support. Hosseini et al. [48] synthesized the nanocomposites of graphene oxide and $MgFe_2O_4$ and observed the phase maintenance of the precursors.

The FAU, $MgFe_2O_4$, and FAU:$MgFe_2O_4$ (3:1) SEM images are shown in Figure 2. FAU has an average size of 0.5 to 1 µm. Ferrite magnetic exhibits agglomerated nanoparticles with a diameter inferior to 50 nm. There is also a high agglomeration degree in $MgFe_2O_4$, usually reported for superparamagnetic compounds, due to the dipolar interactions between the magnetic phases of the nanoparticles [49]. As observed in the FAU:$MgFe_2O_4$ (3:1) image, the FAU appears with smaller particles on its surface, which can be attributed to the presence of $MgFe_2O_4$.

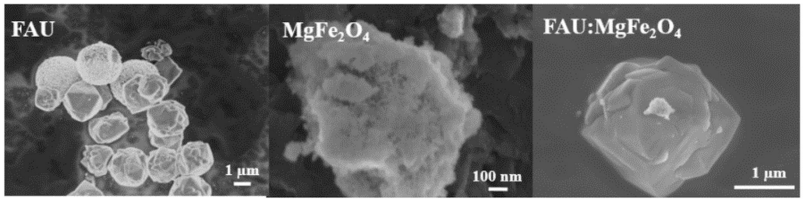

Figure 2. SEM images of FAU, $MgFe_2O_4$, and FAU:$MgFe_2O_4$ (3:1).

$MgFe_2O_4$ distribution on the FAU surface elements for the nanocomposite was mapped using energy-dispersive X-rays via an SEM microscope (SEM-EDS). In Figure 3, the distribution and overlapping of Si and Al refer to the FAU elements. Additionally, Fe and Mg comprise the $MgFe_2O_4$. It can be seen that the ferrite is distributed in an agglomerated form in the zeolite surface regions. Thus, the SEM-EDS images confirm that the magnetic

nanocomposite can be obtained by impregnating the magnetic nanoparticles in the FAU zeolite surface. These results, associated with the X-ray diffractogram (Figure 1), show that the production of the magnetic nanocomposite was successful.

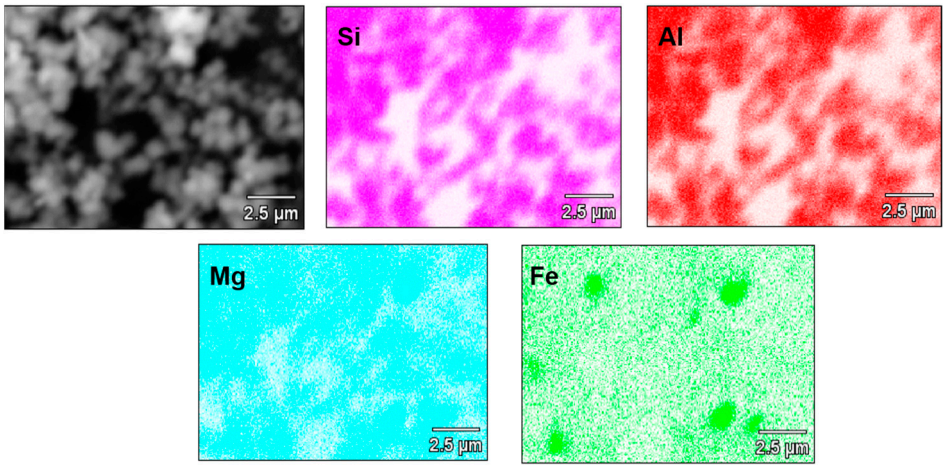

Figure 3. Images of SEM-EDS mapping for FAU:$MgFe_2O_4$ (3:1), showing element distributions.

The values of the micropore volume (V_{Micro}) and total (SSA_{BET}) and external surface (S_{Ext}) areas for the materials are shown in Table 1. A decrease in S_{BET} from 650 m^2 g^{-1} (FAU) to 400 m^2 g^{-1} in the FAU:$MgFe_2O_4$ nanocomposite can be noted. V_{Micro} is verified as having a minimal reduction, from 0.30 cm^3 g^{-1} to 0.20 cm^3 g^{-1}, in the nanocomposite. The values are coherent given the desired material composition, since the nanocomposite was prepared at a ratio of 3:1 FAU:$MgFe_2O_4$ (w w^{-1}), preserving surface properties from the zeolite. This result can be attributed to the agglomeration effect caused by the magnetic nanoparticles. Magnetic particles promote spin orientation that occasions attraction and agglomeration [50].

Table 1. N_2 physisorption analysis through the BET mathematical model of FAU, $MgFe_2O_4$, and FAU:$MgFe_2O_4$ samples.

Sample	S_{Ext} (m^2 g^{-1})	SSA_{BET} (m^2 g^{-1})	V_{Micro} (cm^3 g^{-1})
FAU	390	650	0.30
$MgFe_2O_4$	14	19	0.051
FAU:$MgFe_2O_4$	34	400	0.20

Magnetic curves were analyzed in order to understand the $MgFe_2O_4$ magnetic behavior (Figure 4). The results presented in Figure 4 show that $MgFe_2O_4$ presents 5.90 emu g^{-1} for saturation magnetization (Ms) and 0.10 emu g^{-1} for remaining magnetization (Mr). A similar result was obtained by Sheykhan et al. [51] for $MgFe_2O_4$ synthesized via the coprecipitation method and calcined at 550 °C for 6 h. The authors observed a Ms value of 6.00 emu g^{-1} and Mr of 0.0008 emu g^{-1}. Figure 4a shows the typical behavior slope for materials with soft magnetic nature, as widely reported in the literature [52–55]. The narrow shape of the curves also demonstrates that the material can be readily demagnetized, affirming its superparamagnetic nature [56]. When analyzing the FAU:$MgFe_2O_4$ (3:1) nanocomposite's magnetic capacity, a decrease in Ms from 5.90 to 0.47 emu g^{-1} and Mr from 0.10 to 0.01 emu g^{-1} (Figure 4b) is observed. Paris et al. [57] prepared Nb_2O_5:$MgFe_2O_4$ magnetic photocatalysts, obtaining a Ms of 3 emu g^{-1}. This study showed a decrease in magnetization compared to pure magnetic material due to the content of magnetic nanoparticles in the composite. Su et al. [58] studied the ZnO:$MgFe_2O_4$ (1:1) composite. A decrease in Ms from 40 to 20 emu g^{-1} for the ferrite in the nanocomposite form was observed. The reduction in the nanocomposite magnetic effect concerning isolated ferrite corresponded to

the ratio used, which was equivalent to 25%. This result corresponds to the present work, since FAU zeolite in the nanocomposite consists of a non-magnetic component.

As shown in Figure 4c, the developed system can be removed after adsorption with a magnet at the laboratory scale or projected via the appliance in natural environmental conditions, according to the applied magnetic field. In addition, it is worth mentioning that the main advantage of resorting to $MgFe_2O_4$ is its low toxicity, especially when compared to other ferrites, such as ferrites that contain cobalt [59–61], since Fe and Mg ions are soil nutrients.

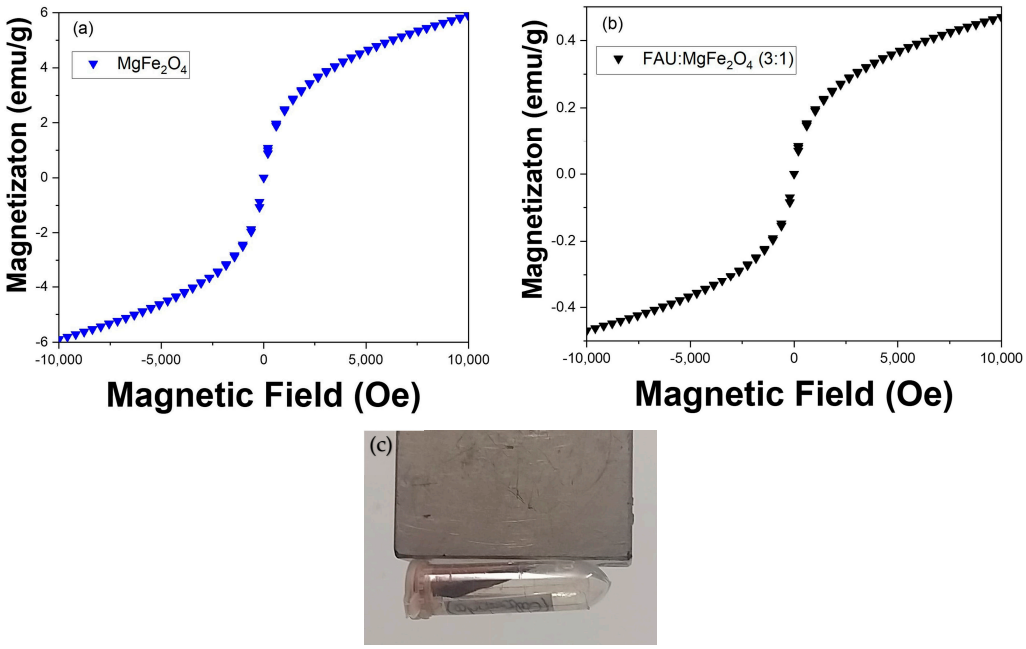

Figure 4. Magnetic curves: (**a**) $MgFe_2O_4$; (**b**) FAU:$MgFe_2O_4$; and (**c**) image of soft magnetic $MgFe_2O_4$ ferrite.

Concerning the nanocomposites, as observed in Figure 4, in terms of magnetic behavior, in the evaluated FAU:$MgFe_2O_4$ 3:1 (w w^{-1}) proportion, the weak properties and the low values contributed to the difficulty of complete separation in an aqueous medium. As seen in Figure 5a, the nanocomposite is attracted to the magnetic in dry form (Figure 5a (left)) and an aqueous medium (Figure 5a (right)). However, the nanocomposite in a 3:1 ratio (w w^{-1}) does not allow the complete attraction of particles (turbidity), keeping it partially separated in suspension. The nanocomposite magnetic capacity was evaluated via mass recovery through five cycles using a neodymium magnet (Figure 5b). At the end of the first cycle, the weight decreased from 0.1 g to 0.039 ± 0.004 g, corresponding to around 60% recovery. It is noticed that the recovery percentage after the 1st cycle remained very similar until the fifth cycle. In the present system, FAU:$MgFe_2O_4$ at a ratio of 3:1 (w w^{-1}) would be necessary to increase the proportion of magnesium ferrite in the nanocomposite for a better magnetical response. However, recovering approximately 60% of the adsorbent in the evaluated conditions is possible.

The adsorption assays of Mn^{2+} and Co^{2+} ions were carried out in an aqueous medium at 10, 50, and 100 mg L^{-1}, using the nanocomposite FAU:$MgFe_2O_4$ at different dosages (0.25, 0.5, and 1.0 g L^{-1}) for 24 h. Figure 6 shows the graphs of the adsorption test results.

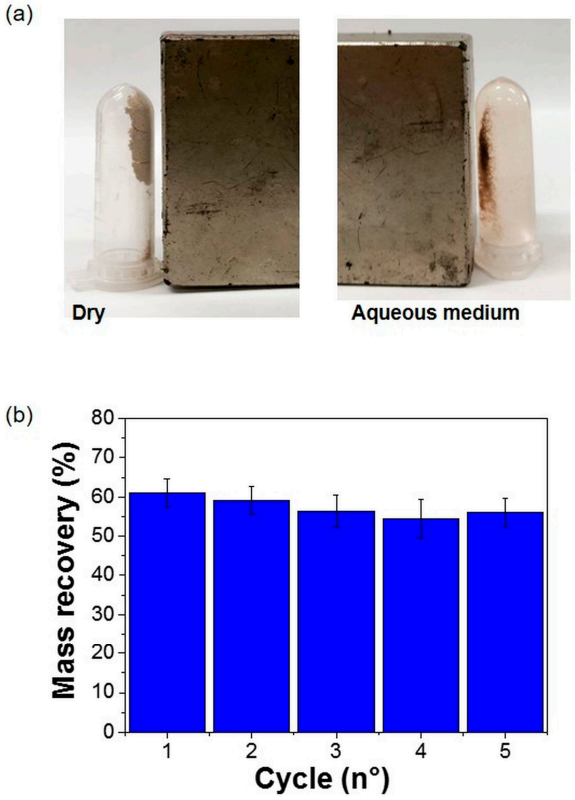

Figure 5. FAU:$MgFe_2O_4$ (3:1) magnetic attraction: (**a**) dried (left) and aqueous medium (right); (**b**) mass recovery through neodymium magnetic.

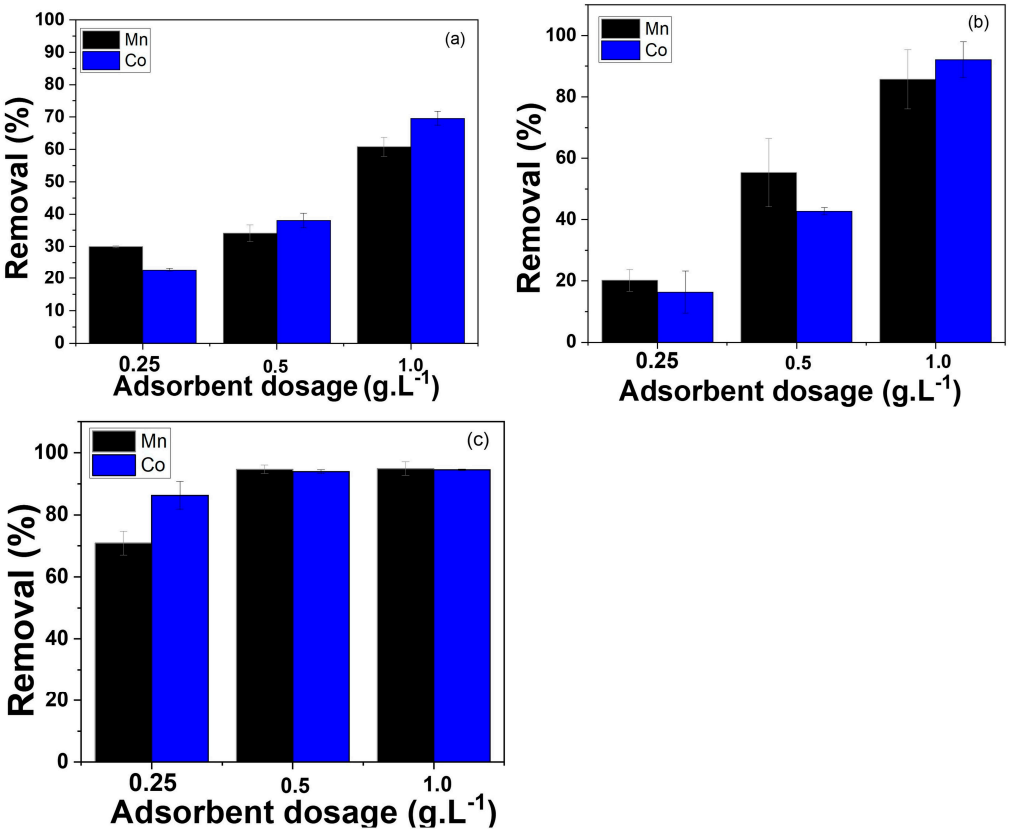

Figure 6. Adsorption assays using FAU:$MgFe_2O_4$ (0.25, 0,5, and 1.0 g L^{-1} dosages) over 24 h for Co^{2+} and Mn^{2+} ions concentrations: (**a**) 100 mg L^{-1}; (**b**) 50 mg L^{-1}; (**c**) 10 mg L^{-1}.

Concerning Figure 6, the adsorption test results showed that for a contaminant concentration of 10 mg L^{-1}, the highest adsorption percentages are 94.5% and 94.9% for the Co^{2+} and Mn^{2+} ions, respectively, using a nanocomposite dosage of 1.0 g L^{-1}.

Two interesting trends were observed in Figure 6. First, the removal percentage increased with increasing adsorbent dosage for a particular contaminant ion concentration. This behavior is due to the increase in the adsorbent dosage increasing the number of adsorption sites. The second trend is that the removal percentage increased with the decreasing contaminant ion concentrations. This can be explained by the fact that, for a fixed adsorbent dosage, there is a certain number of available adsorption sites in the FAU:$MgFe_2O_4$. So, for more diluted solutions, it is possible to adsorb as many contaminant ions as possible without filling up all the available adsorption sites. Then, as the contaminant ions concentration increases, more contaminant ions will be present on the same number of adsorption sites, leading to a lower removal percentage [62].

Paris et al. [50] evaluated the Pb^{2+} ion removal with a nanocomposite of faujasite zeolite and magnesium/cobalt ferrite, also at a 3:1 ratio (w w^{-1}). The authors stated that the nanocomposite removed 99% of Pb^{2+} in an aqueous medium, demonstrating high efficiency.

The kinetics study provided information on the adsorption capacity in an aqueous medium as a function of time. Therefore, the best removal results of the adsorption assays were used. The conditions for the kinetic evaluation were 10 mg L^{-1} of the contaminant in contact with 1.0 g L^{-1} of FAU:$MgFe_2O_4$. Figure 7 presents graphs depicting the kinetic assay with varying adsorption times.

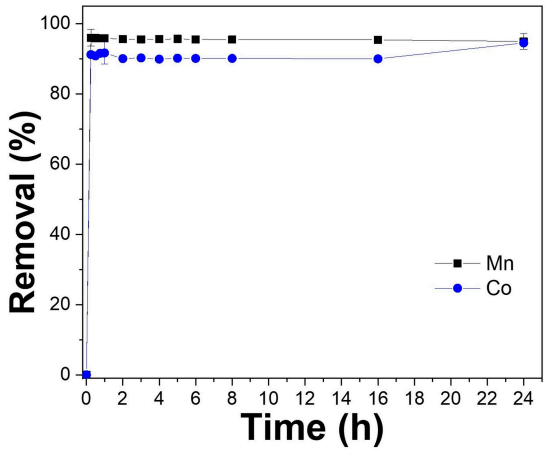

Figure 7. Kinetic assays: the adsorption of Co^{2+} and Mn^{2+} ions using 1 g L^{-1} of the FAU:$MgFe_2O_4$ nanocomposite versus time.

Under the evaluated conditions, the adsorption/desorption equilibrium is reached in the first 15 min (0.25 h) of contact between the adsorbent (FAU:$MgFe_2O_4$) and the adsorbate (metallic ions). For Mn^{2+} and Co^{2+}, respectively, approximately 95% and 94% of these contaminants were removed, remaining constant until the end of the test.

The kinetic model's pseudo-first order and pseudo-second order results were evaluated. Figure 8 and Table 2 represent the fits of the models considered.

The results of the kinetic evaluation show that the removal of ions is high in the initial stages of adsorption and reaches equilibrium quickly. According to Reference [22], it is known that the adsorption process occurs preferentially on the surface of the FAU via ion exchange. The R^2 parameter showed that pseudo-first and pseudo-second order models adjusted for the adsorption kinetics in these assays are comparable, meaning that either model could satisfactorily explain the kinetic data of this situation. The parameters determined by the models are 3.88 and 3.58 mg g^{-1} for Co^{2+} and Mn^{2+}, respectively. Liu et al. [63] synthesized zeolite Y and studied the adsorption kinetics of toxic metal ions, such as Co^{2+} and Ni^{2+}. The authors performed nonlinear kinetic adjustments and verified that

both kinetic models, pseudo-first and n-th order reactions, adequately described the kinetic adsorption behavior.

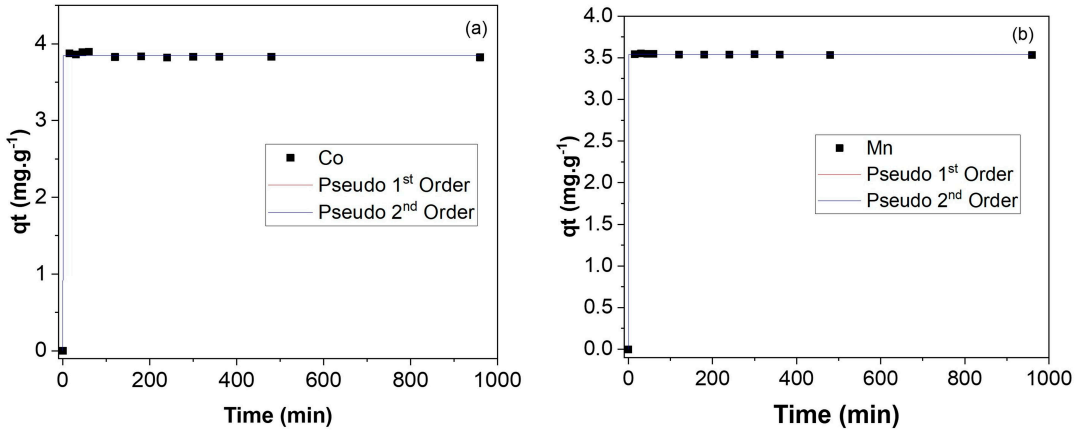

Figure 8. Pseudo-first and -second order models for Co^{2+} (**a**) and Mn^{2+} (**b**) adsorption. Concentrations: 10 mg L^{-1} of metallic ions and a 1.0 g L^{-1} dosage of FAU:$MgFe_2O_4$.

Table 2. The parameters of nonlinear kinetic models considering pseudo-first and pseudo-second order values for Co^{2+} (a) and Mn^{2+} ions (b). Concentrations: 10 mg L^{-1} of metallic ions and a 1.0 g L^{-1} dosage of FAU:$MgFe_2O_4$.

Model	Parameter	Value	
		Co (a)	**Mn (b)**
Pseudo-First Order	R^2	0.99941	0.99998
	k_1 (min^{-1})	7.89×10^3	8.80×10^2
	qe	3.85	3.54
Pseudo-Second Order	R^2	0.99941	0.99997
	k_2 (g mg^{-1} min^{-1})	1.02×10^{20}	1.08×10^{19}
	qe	3.85	3.54

Finally, the reusability of the nanocomposite FAU:$MgFe_2O_4$ was evaluated. In this reuse test, the material was separated via centrifugation after 24 h of contact with contaminating ions. Three reuse cycles were performed, and Figure 9 shows the behavior seen in the tests.

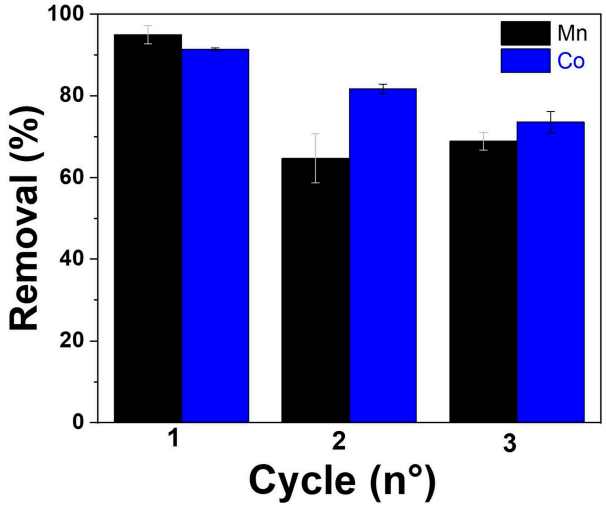

Figure 9. Reuse assays of the Co^{2+} and Mn^{2+} ions (10 mg L^{-1}) for 24 h with FAU:$MgFe_2O_4$ (1 g L^{-1}).

The material proved to be efficient in the reuse tests. In the first cycle, the FAU:$MgFe_2O_4$ removed 91.3% of Co^{2+} and 85.3% of Mn^{2+}. The adsorption percentage decreases with reuse, as expected. In the third cycle, the nanocomposite removed 73.5% and 68.8% of Co^{2+} and Mn^{2+} ions, respectively. This decrease can be attributed to saturation ions on the zeolite surface, minimizing active sites. The results indicate that the nanocomposite can be reused as an adsorbent.

Furthermore, zeolites present stability mainly when subjected to hydrothermal treatments [64], as in this work. The hydrothermal treatment used for synthesis causes chemical changes that ensure zeolite structure stability at different pHs and temperatures [65]. Thus, the structural maintenance of zeolites makes it possible for this material to be reused. Therefore, the magnetic nanocomposite is able to treat water contaminated by toxic metal ions in routine activities. After waste treatment, a magnet is able to attract the adsorbent and separate it from the aqueous medium. Additionally, from an analytical perspective [66,67], the adsorbent enables ion availability, facilitating ion analyses.

4. Conclusions

The FAU:$MgFe_2O_4$ (3:1) nanocomposite was obtained, maintaining the integrity of the precursors, faujasite zeolite and magnesium ferrite. The material demonstrated soft superparamagnetic characteristics, possibly able to remove the nanocomposite after adsorption. In the adsorption tests with 1.0 g L^{-1} of FAU:$MgFe_2O_4$ and 10 mg L^{-1} of contaminant concentration, the nanocomposite showed the efficient removal of the ions, with 94.5% for Co^{2+} and 94.9% for Mn^{2+}. The FAU:$MgFe_2O_4$ nanocomposite displayed reuse capacity, supplying adsorption values of higher than 65% in the third cycle for both ions. The mass magnetical recovery evaluation demonstrated a 60% capacity until the fifth cycle. In this way, the FAU:$MgFe_2O_4$ nanocomposite is a promising alternative for removing metallic ions in polluted water, promoting recovery and reuse.

Author Contributions: Conceptualization, M.R.M., J.O.D.M. and E.C.P.; methodology, M.R.M. and J.O.D.M.; software, M.R.M.; validation, A.H.P. and E.C.P.; formal analysis, M.T.E. and A.H.P.; investigation, M.R.M.; resources, E.C.P.; data curation, J.O.D.M., A.H.P. and E.C.P.; writing—original draft preparation, M.R.M. and J.O.D.M.; writing—review and editing, M.R.M., J.O.D.M., A.H.P. and E.C.P.; visualization, J.O.D.M. and E.C.P.; supervision, E.C.P.; project administration, E.C.P.; funding acquisition, E.C.P. All authors have read and agreed to the published version of the manuscript.

Funding: This study was financed in part by the Coordenação de Aperfeiçoamento de Pessoal de Nível Superior—Brasil (CAPES)—Finance Code 001. São Paulo Research Foundation (FAPESP) (Grant Number 2021/14992-1). The authors acknowledge Embrapa (Grant Number 11.14.03.001.01.00), CNPq (grant number 461384/2014-0 and PIBIC grant number 127989/2020-0), Financiadora de Estudos e Projetos (FINEP), Sistema Nacional de Laboratórios em Nanotecnologias (SisNano), and Rede de Nanotecnolgia Aplicada ao Agronegócio (AgroNano Network) for financial support.

Institutional Review Board Statement: Not applicable.

Informed Consent Statement: Not applicable.

Data Availability Statement: Not applicable.

Conflicts of Interest: The authors declare no conflict of interest.

References

1. Paris, E.C.; Malafatti, J.O.D.; Moreira, A.J.; Santos, L.C.; Sciena, C.R.; Zenatti, A.; Escote, M.T.; Mastelaro, V.R.; Joya, M.R. CuO nanoparticles decorated on hydroxyapatite/ferrite magnetic support: Photocatalysis, cytotoxicity, and antimicrobial response. *Environ. Sci. Pollut. Res.* **2022**, *29*, 41505–41519. [CrossRef]
2. Baines, C.; Lerebours, A.; Thomas, F.; Fort, J.; Kreitsberg, R.; Gentes, S.; Meitern, R.; Saks, L.; Ujvari, B.; Giraudeau, M. Linking pollution and cancer in aquatic environments: A review. *Environ. Int.* **2021**, *149*, 106391. [CrossRef] [PubMed]
3. Malafatti, J.O.; Moreira, A.J.; Sciena, C.R.; Silva, T.E.; Freschi, G.P.; Pereira, E.C.; Paris, E.C. Prozac® removal promoted by HAP: Nb_2O_5 nanoparticles system: By-products, mechanism, and cytotoxicity assessment. *J. Environ. Chem. Eng.* **2021**, *9*, 104820. [CrossRef]

4. Schwarzenbach, R.P.; Egli, T.; Hofstetter, T.B.; Von Gunten, U.; Wehrli, B. Global water pollution and human health. *Annu. Rev. Environ. Resour.* **2010**, *35*, 109–136. [CrossRef]
5. Prabhu, P.P.; Prabhu, B. (Eds.) A review on removal of heavy metal ions from waste water using natural/modified bentonite. In Proceedings of the MATEC Web of Conferences, Osaka, Japan, 21–22 September 2018; EDP Sciences: Les Ulis, France, 2018.
6. Briffa, J.; Sinagra, E.; Blundell, R. Heavy metal pollution in the environment and their toxicological effects on humans. *Heliyon* **2020**, *6*, e04691. [CrossRef]
7. Rincón Joya, M.; Barba Ortega, J.; Malafatti, J.O.D.; Paris, E.C. Evaluation of photocatalytic activity in water pollutants and cytotoxic response of α-Fe_2O_3 nanoparticles. *ACS Omega* **2019**, *4*, 17477–17486. [CrossRef]
8. Yousefi, Z.; Zazouli, M. Removal of heavy metals from solid wastes leachates coagulation-flocculation process. *J. Appl. Sci.* **2008**, *8*, 2142–2147. [CrossRef]
9. Trivunac, K.; Stevanovic, S. Removal of heavy metal ions from water by complexation-assisted ultrafiltration. *Chemosphere* **2006**, *64*, 486–491. [CrossRef]
10. Wu, R. Removal of heavy metal ions from industrial wastewater based on chemical precipitation method. *Ekoloji* **2019**, *28*, 2443–2452.
11. Tran, T.-K.; Chiu, K.-F.; Lin, C.-Y.; Leu, H.-J. Electrochemical treatment of wastewater: Selectivity of the heavy metals removal process. *Int. J. Hydrogen Energy* **2017**, *42*, 27741–27748. [CrossRef]
12. Lakherwal, D. Adsorption of heavy metals: A review. *Int. J. Environ. Res. Dev.* **2014**, *4*, 41–48.
13. Salame, I.I.; Bandosz, T.J. Role of surface chemistry in adsorption of phenol on activated carbons. *J. Colloid Interface Sci.* **2003**, *264*, 307–312. [CrossRef] [PubMed]
14. Lima, R.; Espinosa, J.; Gurgel, M.; Paris, E.; Leite, E.; Joya, M.; Pizani, P.; Varela, J.A.; Longo, E. Photoluminescence in disordered Sm-doped Pb Ti O 3: Experimental and theoretical approach. *J. Appl. Phys.* **2006**, *100*, 034917. [CrossRef]
15. Chaouati, N.; Soualah, A.; Chater, M. Adsorption of phenol from aqueous solution onto zeolites Y modified by silylation. *Comptes Rendus Chim.* **2013**, *16*, 222–228. [CrossRef]
16. Lopes, M.M.; Coutinho, T.C.; Malafatti, J.O.D.; Paris, E.C.; de Sousa, C.P.; Farinas, C.S. Immobilization of phytase on zeolite modified with iron (II) for use in the animal feed and food industry sectors. *Process Biochem.* **2021**, *100*, 260–271. [CrossRef]
17. Taylor, W. The nature and properties of aluminosilicate framework structures. *Proc. R. Soc. Lond. Ser. A Contain. Pap. A Math. Phys. Character* **1934**, *145*, 80–103.
18. Payra, P.; Dutta, P.K. Zeolites: A primer. In *Handbook of Zeolite Science and Technology*; CRC Press: Boca Raton, USA, 2003; pp. 1–24.
19. Reinoso, D.; Adrover, M.; Pedernera, M. Green synthesis of nanocrystalline faujasite zeolite. *Ultrason. Sonochem.* **2018**, *42*, 303–309. [CrossRef]
20. Liu, C.; Li, G.; Hensen, E.J.; Pidko, E.A. Relationship between acidity and catalytic reactivity of faujasite zeolite: A periodic DFT study. *J. Catal.* **2016**, *344*, 570–577. [CrossRef]
21. Rouquerol, J.; Llewellyn, P.; Sing, K. Adsorption by clays, pillared clays, zeolites and aluminophosphates. In *Adsorption by Powders and Porous Solids Principles Methodology and Applications*; Academic Press: Amsterdam, The Netherlands, 2014; pp. 467–527.
22. Jeffroy, M.; Boutin, A.; Fuchs, A.H. Understanding the equilibrium ion exchange properties in faujasite zeolite from Monte Carlo simulations. *J. Phys. Chem. B* **2011**, *115*, 15059–15066. [CrossRef]
23. Coutinho, T.C.; Malafatti, J.O.; Paris, E.C.; Tardioli, P.W.; Farinas, C.S. Hydroxyapatite-$CoFe_2O_4$ magnetic nanoparticle composites for industrial enzyme immobilization, use, and recovery. *ACS Appl. Nano Mater.* **2020**, *3*, 12334–12345. [CrossRef]
24. Alshorifi, F.T.; Alswat, A.A.; Salama, R.S. Gold-selenide quantum dots supported onto cesium ferrite nanocomposites for the efficient degradation of rhodamine B. *Heliyon* **2022**, *8*, e09652. [CrossRef] [PubMed]
25. Oliveira, L.C.; Petkowicz, D.I.; Smaniotto, A.; Pergher, S.B. Magnetic zeolites: A new adsorbent for removal of metallic contaminants from water. *Water Res.* **2004**, *38*, 3699–3704. [CrossRef] [PubMed]
26. Cao, J.-L.; Liu, X.-W.; Fu, R.; Tan, Z.-Y. Magnetic P zeolites: Synthesis, characterization and the behavior in potassium extraction from seawater. *Sep. Purif. Technol.* **2008**, *63*, 92–100. [CrossRef]
27. Supelano, G.; Cuaspud, J.G.; Moreno-Aldana, L.C.; Ortiz, C.; Trujillo, C.; Palacio, C.; Vargas, C.P.; Gómez, J.M. Synthesis of magnetic zeolites from recycled fly ash for adsorption of methylene blue. *Fuel* **2020**, *263*, 116800. [CrossRef]
28. Loiola, A.R.; Bessa, R.A.; Oliveira, C.P.; Freitas, A.D.; Soares, S.A.; Bohn, F.; Pergher, S.B. Magnetic zeolite composites: Classification, synthesis routes, and technological applications. *J. Magn. Magn. Mater.* **2022**, *560*, 169651. [CrossRef]
29. Fungaro, D.A.; Yamaura, M.; Graciano, J.E.A. Remoção de íons Zn^{2+}, Cd^{2+} e Pb^{2+} de soluções aquosas usando compósito magnético de zeólita de cinzas de carvão. *Química Nova* **2010**, *33*, 1275–1278. [CrossRef]
30. Xian, G.; Kong, S.; Li, Q.; Zhang, G.; Zhou, N.; Du, H.; Niu, L. Synthesis of spinel ferrite MFe_2O_4 (M = Co, Cu, Mn, and Zn) for persulfate activation to remove aqueous organics: Effects of M-site metal and synthetic method. *Front. Chem.* **2020**, *8*, 177. [CrossRef] [PubMed]
31. Hakeem, A.; Alshahrani, T.; Muhammad, G.; Alhossainy, M.; Laref, A.; Khan, A.R.; Ali, I.; Farid, H.M.T.; Ghrib, T.; Ejaz, S.R. Magnetic, dielectric and structural properties of spinel ferrites synthesized by sol-gel method. *J. Mater. Res. Technol.* **2021**, *11*, 158–169. [CrossRef]
32. Masunga, N.; Mamba, B.B.; Getahun, Y.W.; El-Gendy, A.A.; Kefeni, K.K. Synthesis of single-phase superparamagnetic copper ferrite nanoparticles using an optimized coprecipitation method. *Mater. Sci. Eng. B* **2021**, *272*, 115368. [CrossRef]

33. Nguyen, L.T.; Nguyen, L.T.; Manh, N.C.; Quoc, D.N.; Quang, H.N.; Nguyen, H.T.; Nguyen, D.C.; Bach, L.G. A facile synthesis, characterization, and photocatalytic activity of magnesium ferrite nanoparticles via the solution combustion method. *J. Chem.* **2019**, *2019*, 3428681. [CrossRef]
34. Fayazzadeh, S.; Khodaei, M.; Arani, M.; Mahdavi, S.; Nizamov, T.; Majouga, A. Magnetic properties and magnetic hyperthermia of cobalt ferrite nanoparticles synthesized by hydrothermal method. *J. Supercond. Nov. Magn.* **2020**, *33*, 2227–2233. [CrossRef]
35. Liu, B.; Wang, Y.; Han, G.; Zhang, L.; Huang, Y. Facile microwave-assisted synthesis of magnetic ferrite: Rapid interfacial reaction underlying intensifying mechanism. *J. Clean. Prod.* **2022**, *361*, 132181. [CrossRef]
36. Ateia, E.E.; Ateia, M.A.; Fayed, M.G.; El-Hout, S.I.; Mohamed, S.G.; Arman, M. Synthesis of nanocubic lithium cobalt ferrite toward high-performance lithium-ion battery. *Appl. Phys. A* **2022**, *128*, 483. [CrossRef]
37. Fang, X.; Ma, D.; Sun, B.; Xu, X.; Quan, W.; Xiao, Z.; Zhai, Y. A high-performance magnetic shield with MnZn ferrite and Mu-metal film combination for atomic sensors. *Materials* **2022**, *15*, 6680. [CrossRef] [PubMed]
38. Gupta, R.; Singh, S.; Walia, R.; Kumar, V.; Verma, V. Modification in photovoltaic and photocatalytic properties of bismuth ferrites by tailoring band-gap and ferroelectric properties. *J. Alloys Compd.* **2022**, *908*, 164602. [CrossRef]
39. Uddin, M.J.; Jeong, Y.-K. Application of magnesium ferrite nanomaterials for adsorptive removal of arsenic from water: Effects of Mg and Fe ratio. *Chemosphere* **2022**, *307*, 135817. [CrossRef]
40. Reddy, S.; Swamy, B.K.; Chandra, U.; Mahathesha, K.; Sathisha, T.; Jayadevappa, H. Synthesis of $MgFe_2O_4$ nanoparticles and $MgFe_2O_4$ nanoparticles/CPE for electrochemical investigation of dopamine. *Anal. Methods* **2011**, *3*, 2792–2796. [CrossRef]
41. Kurian, J.; Mathew, M.J. Structural, magnetic and mossbauer studies of magnesium ferrite nanoparticles prepared by hydrothermal method. *Int. J. Nanosci.* **2018**, *17*, 1760001. [CrossRef]
42. Nonkumwong, J.; Pakawanit, P.; Wipatanawin, A.; Jantaratana, P.; Ananta, S.; Srisombat, L. Synthesis and cytotoxicity study of magnesium ferrite-gold core-shell nanoparticles. *Mater. Sci. Eng. C* **2016**, *61*, 123–132. [CrossRef]
43. Peng, Z.-D.; Lin, X.-M.; Zhang, Y.-L.; Hu, Z.; Yang, X.-J.; Chen, C.-Y.; Chen, H.-Y.; Li, Y.-T.; Wang, J.-J. Removal of cadmium from wastewater by magnetic zeolite synthesized from natural, low-grade molybdenum. *Sci. Total Environ.* **2021**, *772*, 145355. [CrossRef]
44. Neolaka, Y.A.; Lawa, Y.; Naat, J.; Riwu, A.A.; Mango, A.W.; Darmokoesoemo, H.; Widyaningrum, B.A.; Iqbal, M.; Kusuma, H.S. Efficiency of activated natural zeolite-based magnetic composite (ANZ-Fe_3O_4) as a novel adsorbent for removal of Cr (VI) from wastewater. *J. Mater. Res. Technol.* **2022**, *18*, 2896–2909. [CrossRef]
45. Mthombeni, N.H.; Onyango, M.S.; Aoyi, O. Adsorption of hexavalent chromium onto magnetic natural zeolite-polymer composite. *J. Taiwan Inst. Chem. Eng.* **2015**, *50*, 242–251. [CrossRef]
46. Omer, M.I.; Elbadawi, A.; Yassin, O. Synthesis and structural properties of $MgFe_2O_4$ ferrite nano-particles. *J. Appl. Ind. Sci.* **2013**, *1*, 20–23.
47. Yamaura, M.; Fungaro, D.A. Synthesis and characterization of magnetic adsorbent prepared by magnetite nanoparticles and zeolite from coal fly ash. *J. Mater. Sci.* **2013**, *48*, 5093–5101. [CrossRef]
48. Hosseini, S.A.; Talebipour, S.; Neyestani, M.R.; Ranjan, S.; Dasgupta, N. Graphene oxide $MgFe_2O_4$ nanocomposites for Cr (VI) remediation: A comparative modeling study. *Nanotechnol. Environ. Eng.* **2018**, *3*, 10. [CrossRef]
49. Pedrosa, S.; Martins, S., Jr.; Souza, R.; Dantas, J.; Souza, C.; Rebouças, G.; De Araújo, J.; Dantas, A.L.; Carriço, A. Dipolar effects on the magnetic phases of superparamagnetic clusters. *J. Appl. Phys.* **2018**, *123*, 233902. [CrossRef]
50. Paris, E.C.; Malafatti, J.O.; Musetti, H.C.; Manzoli, A.; Zenatti, A.; Escote, M.T. Faujasite zeolite decorated with cobalt ferrite nanoparticles for improving removal and reuse in Pb^{2+} ions adsorption. *Chin. J. Chem. Eng.* **2020**, *28*, 1884–1890. [CrossRef]
51. Sheykhan, M.; Mohammadnejad, H.; Akbari, J.; Heydari, A. Superparamagnetic magnesium ferrite nanoparticles: A magnetically reusable and clean heterogeneous catalyst. *Tetrahedron Lett.* **2012**, *53*, 2959–2964. [CrossRef]
52. Bamzai, K.; Kour, G.; Kaur, B.; Kulkarni, S. Effect of cation distribution on structural and magnetic properties of Dy substituted magnesium ferrite. *J. Magn. Magn. Mater.* **2013**, *327*, 159–166. [CrossRef]
53. Feng, Y.; Li, S.; Zheng, Y.; Yi, Z.; He, Y.; Xu, Y. Preparation and characterization of MgFe2O4 nanocrystallites via PVA sol-gel route. *J. Alloys Compd.* **2017**, *699*, 521–525. [CrossRef]
54. Huang, Y.; Tang, Y.; Wang, J.; Chen, Q. Synthesis of $MgFe_2O_4$ nanocrystallites under mild conditions. *Mater. Chem. Phys.* **2006**, *97*, 394–397. [CrossRef]
55. Da Dalt, S.; Bergmann, C. Thermal, Structural and Magnetic Behavior of the $MgFe_2O_4$ Nanostructured. In Proceedings of the IBEROMET XIX CONAMET/SAM, Viña del Mar, Chile, 2–5 November 2010; Redalyc: Ciudad de México, Mexico, 2010; pp. 1–7.
56. Naaz, F.; Dubey, H.K.; Kumari, C.; Lahiri, P. Structural and magnetic properties of $MgFe_2O_4$ nanopowder synthesized via co-precipitation route. *SN Appl. Sci.* **2020**, *2*, 808. [CrossRef]
57. Paris, E.C.; Malafatti, J.O.D.; Sciena, C.R.; Junior, L.F.N.; Zenatti, A.; Escote, M.T.; Moreira, A.J.; Freschi, G.P.G. Nb_2O_5 nanoparticles decorated with magnetic ferrites for wastewater photocatalytic remediation. *Environ. Sci. Pollut. Res.* **2021**, *28*, 23731–23741. [CrossRef] [PubMed]
58. Su, N.R.; Lv, P.; Li, M.; Zhang, X.; Li, M.; Niu, J. Fabrication of $MgFe_2O_4$–ZnO heterojunction photocatalysts for application of organic pollutants. *Mater. Lett.* **2014**, *122*, 201–204. [CrossRef]
59. Bose, S.; Tripathy, B.K.; Debnath, A.; Kumar, M. Boosted sono-oxidative catalytic degradation of Brilliant green dye by magnetic $MgFe_2O_4$ catalyst: Degradation mechanism, assessment of bio-toxicity and cost analysis. *Ultrason. Sonochem.* **2021**, *75*, 105592. [CrossRef] [PubMed]

60. Hengstler, J.G.; Bolm-Audorff, U.; Faldum, A.; Janssen, K.; Reifenrath, M.; Götte, W.; Jung, D.; Mayer-Popken, O.; Fuchs, J.; Gebhard, S. Occupational exposure to heavy metals: DNA damage induction and DNA repair inhibition prove co-exposures to cadmium, cobalt and lead as more dangerous than hitherto expected. *Carcinogenesis* **2003**, *24*, 63–73. [CrossRef]
61. Scharf, B.; Clement, C.C.; Zolla, V.; Perino, G.; Yan, B.; Elci, S.G.; Purdue, E.; Goldring, S.; Macaluso, F.; Cobelli, N. Molecular analysis of chromium and cobalt-related toxicity. *Sci. Rep.* **2014**, *4*, 5729. [CrossRef]
62. Fernandes, A.; Almeida, C.; Menezes, C.; Debacher, N.; Sierra, M. Removal of methylene blue from aqueous solution by peat. *J. Hazard. Mater.* **2007**, *144*, 412–419. [CrossRef] [PubMed]
63. Liu, Y.; Wang, G.; Luo, Q.; Li, X.; Wang, Z. The thermodynamics and kinetics for the removal of copper and nickel ions by the zeolite Y synthesized from fly ash. *Mater. Res. Express* **2018**, *6*, 025001. [CrossRef]
64. Simancas, R.; Chokkalingam, A.; Elangovan, S.P.; Liu, Z.; Sano, T.; Iyoki, K.; Wakihara, T.; Okubo, T. Recent progress in the improvement of hydrothermal stability of zeolites. *Chem. Sci.* **2021**, *12*, 7677–7695. [CrossRef]
65. Heard, C.J.; Grajciar, L.; Uhlík, F.; Shamzhy, M.; Opanasenko, M.; Čejka, J.; Nachtigall, P. Zeolite (in) stability under aqueous or steaming conditions. *Adv. Mater.* **2020**, *32*, 2003264. [CrossRef] [PubMed]
66. Condomitti, U.; Zuin, A.; Silveira, A.T.; Araki, K.; Toma, H.E. Direct use of superparamagnetic nanoparticles as electrode modifiers for the analysis of mercury ions from aqueous solution and crude petroleum samples. *J. Electroanal. Chem.* **2011**, *661*, 72–76. [CrossRef]
67. Liosis, C.; Papadopoulou, A.; Karvelas, E.; Karakasidis, T.E.; Sarris, I.E. Heavy metal adsorption using magnetic nanoparticles for water purification: A critical review. *Materials* **2021**, *14*, 7500. [CrossRef] [PubMed]